International Journal of Nanomedicine

Dovepress
open access to scientific and medical research

Open Access Full Text Article

ORIGINAL RESEARCH

Exceedingly biocompatible and thin-layered reduced graphene oxide nanosheets using an eco-friendly mushroom extract strategy

This article was published in the following Dove Press journal:
International Journal of Nanomedicine
20 February 2015
Number of times this article has been viewed

Kasturi Muthoosamy[1]
Renu Geetha Bai[1]
Ibrahim Babangida Abubakar[2]
Surya Mudavasseril Sudheer[1]
Hong Ngee Lim[3]
Hwei-San Loh[2,4]
Nay Ming Huang[5]
Chin Hua Chia[6]
Sivakumar Manickam[1]

[1]Manufacturing and Industrial Processes Research Division, Faculty of Engineering, [2]School of Biosciences, Faculty of Science, University of Nottingham Malaysia Campus, Semenyih, Selangor, Malaysia; [3]Department of Chemistry, Faculty of Science, Universiti Putra Malaysia, Serdang, Selangor, Malaysia; [4]Biotechnology Research Centre, University of Nottingham Malaysia Campus, Semenyih, Selangor, Malaysia; [5]Low Dimension Materials Research Centre, Department of Physics, Faculty of Science, University of Malaya, Kuala Lumpur, Malaysia; [6]School of Applied Physics, Faculty of Science and Technology, Universiti Kebangsaan Malaysia, Bangi, Selangor, Malaysia

Correspondence: Sivakumar Manickam
Manufacturing and Industrial Processes Research Division, Faculty of Engineering, University of Nottingham Malaysia Campus, Jalan Broga, 43500 Semenyih, Selangor, Malaysia
Tel +60 3 8924 8156
Fax +60 3 8924 8017
Email sivakumar.manickam@nottingham.edu.my

Purpose: A simple, one-pot strategy was used to synthesize reduced graphene oxide (RGO) nanosheets by utilizing an easily available over-the-counter medicinal and edible mushroom, *Ganoderma lucidum*.

Methods: The mushroom was boiled in hot water to liberate the polysaccharides, the extract of which was then used directly for the reduction of graphene oxide. The abundance of polysaccharides present in the mushroom serves as a good reducing agent. The proposed strategy evades the use of harmful and expensive chemicals and avoids the typical tedious reaction methods.

Results: More importantly, the mushroom extract can be easily separated from the product without generating any residual byproducts and can be reused at least three times with good conversion efficiency (75%). It was readily dispersible in water without the need of ultrasonication or any surfactants; whereas 5 minutes of ultrasonication with various solvents produced RGO which was stable for the tested period of 1 year. Based on electrochemical measurements, the followed method did not jeopardize RGO's electrical conductivity. Moreover, the obtained RGO was highly biocompatible to not only colon (HT-29) and brain (U87MG) cancer cells, but was also viable towards normal cells (MRC-5).

Conclusion: Besides being eco-friendly, this mushroom based approach is easily scalable and demonstrates remarkable RGO stability and biocompatibility, even without any form of functionalization.

Keywords: extraction, Ganoderma, RGO, ultrasound

Introduction

Graphene, a monolayer of sp^2 hybridized carbon atoms arranged in a honeycomb lattice, has gained tremendous attention among researchers due to its unique mechanical, electrical, and thermal properties, as well as due to its high surface to volume ratio. Various technological applications have been reported for graphene such as in nanoelectronics, supercapacitors, polymer nanocomposites, drug delivery systems, biosensing, solar cells, memory electronics, optoelectronics, transistor devices, etc.[1,2] However, graphene sheet, also known as reduced graphene oxide (RGO), is hydrophobic and tends to agglomerate irreversibly or even transforms back to graphite due to its van der Waals' interaction and its stronger π–π stacking, which limits its further applications. Therefore, the route of synthesis of RGO is of vital importance to impart stability as most of its unique electrical and mechanical properties are associated only with the individualized graphene sheets.[3–5] In addition, imparting solubility in water is also crucial as a well-dispersed RGO would allow further functionalization and open opportunities for various technological applications.

Several methods have been reported to obtain RGO such as micromechanical cleavage,[6] epitaxial growth,[7] chemical vapor deposition,[8] unzipping of carbon nanotubes (CNTs),[9] and chemical reduction of graphene oxide (GO).[10] Micromechanical method suffers from low productivity which hinders large scale applications;[11] the epitaxial growth method produces graphene with random and uncontrollable thickness;[2] whereas the methods of chemical vapor deposition and unzipping of CNTs involve using several chemicals and lengthy reaction steps, besides being tedious. Hence, much focus has been placed on solution-based reduction of GO which generally produces single to few-layer graphene sheets. Conventional thermal reduction, however, requires higher temperatures and pressures for the removal of intercalated water molecules and oxide functional groups.[11,12] In addition, it requires specific reaction vessels and may cause environmental and economic concerns when large scale production is considered.

Therefore, researchers are more interested in finding out suitable reducing agents. The most commonly used chemical reducing agents are anhydrous hydrazine,[13] hydrazine monohydrate,[14] sodium borohydride,[15] and hydroquinone.[16] These reducing agents are highly toxic, harmful, and explosive. Moreover, hydrazine-reduced graphene tends to agglomerate irreversibly and converts into graphite.[17] Metal/hydrochloric acid reduction is another alternative; however, impurities formed from the residual metal hinders further applications.[18,19]

Recently, reduction of GO using environmentally friendly organic agents such as vitamin C,[20] amino acid,[21] glucose,[22] protein,[23] green tea,[24,25] dextran,[26] bacterial respiration,[27] and *Escherichia coli*[12] have taken a center stage and have been proposed as alternatives. Although these methods are eco-friendly, they demand tedious experimental procedures and require expensive reagents and longer reaction times. Besides, some of these methods introduce foreign materials to RGO that may reduce its purity and limit its further applications. An additional step of sonication is often necessary to produce good dispersion in water. Moreover, incomplete reduction and formation of large graphene aggregates hamper its good electrical conductivity.[28] Most of the reports also claim their suitability for drug delivery; however, cytotoxicity studies on normal healthy cells have never been looked into. Thus, there is an impending demand to develop an easy approach which can produce RGO with good purity but without losing its excellent electrical properties and its biocompatibility.

Ganoderma lucidum (GL), widely known as Reishi in Japan or Ling Zhi in People's Republic of China, has been a popular mushroom often used in many medicinal applications. It is used in the treatment of a variety of ailments such as hypertension, diabetes, hepatitis, cancer, and AIDS.[29] In Asia and North America, usage of this mushroom extends to nutraceuticals and food processing due to many of its astounding properties such as antioxidant, anti-inflammatory, antibacterial, and antiviral.[30,31] One of the interesting properties of this mushroom extract is its high content of polysaccharides which exhibit strong antioxidant properties.[32,33] More specifically, the antioxidant quality is mainly contributed by the high content of glucans, which has been observed more in GL compared to any other *Ganoderma* sp.[31,34,35] Besides polysaccharides being the major components, the GL extract also contains proteins and polyphenols;[29,31] however, the higher content of glucan supersedes the content of the former two, and thus it is safe to assume that the excellent reducing ability is mainly due to the polysaccharides (glucans). In addition to glucans, the presence of reducing sugars such as glucose and galactose in the polysaccharide further contributes to its reducing potential.[36] Moreover, the excellent reducing ability of polysaccharide was also proven by the ability to scavenge DPPH (2,2-diphenyl-1-picrylhydrazyl) radicals well, good antioxidant activity, and chelating ability on ferrous ions.[31,37] Thus, using GL extract as a reducing agent in eco-friendly RGO synthesis is a promising prospect. In addition to this, the polysaccharide is highly soluble in water and does not react with RGO, and as a consequence, a simple ultracentrifugation step can be carried out to separate the reducing agent (extract) after the reaction. Hence, we propose a strategy to produce RGO with the following multitude of benefits: 1) one-step simple synthesis; 2) environmentally friendly process; 3) feasibility to produce in larger quantities, hence economical; 4) high purity with absolute removal of mushroom extract; 5) unperturbed electrical properties; and 6) biocompatibility towards cells.

Our present investigation is different from the recently published work where mushroom was used as a reducing agent for RGO synthesis.[38] The major differences can be seen in terms of method of synthesis and the results obtained. Our method requires only 3 hours of preparation and the whole mushroom was used to prepare the mushroom extract for reduction instead of separating the mycelia, which is cumbersome and takes a total of 17 days to prepare. In addition, our reduction reaction is much simpler, whereby it was conducted for 16 hours using a water bath, allowing for bulk production, instead of subjecting to ultrasonication for 24 hours. According to atomic force microscope (AFM), X-ray diffraction (XRD), and size distribution analysis, the RGO obtained in our case is of 1–2 nm thickness, with 3–5 layers, and 181 nm lateral dimension, respectively, instead of much bigger size and thicker sheets, as reported. Moreover, we have carried out the biocompatibility studies both with cancer cells and normal cells, compared to

other reports in which only cytotoxicity studies on cancer cells were determined, disregarding the effects of their synthesized RGO on normal cells, which is crucial, especially for drug-delivery or biomedical applications.

Experiment

Materials

Graphite was purchased from Asbury Graphite Mills, Inc. (Asbury, NJ, USA). GL (commercial grade) was contributed by Ganofarm Sdn. Bhd. (Tanjung Sepat, Malaysia). Typically, mushrooms (including stalk, gills, and cap) were dried and ground into powder form and sold to the commercial market. Other reagents employed were of analytical grade and used as-received. Anhydrous D-glucose was purchased from Thermo Fisher Scientific (Waltham, MA, USA) and phosphate-buffered saline was obtained from Sigma-Aldrich Co. (St Louis, MO, USA). Ultrapure deionized water was obtained from a Milli-Q Plus system (EMD Millipore, Billerica, MA, USA).

Characterization

The reduction of GO was monitored by measuring the ultraviolet–visible (UV–Vis) spectrum of the reaction at predetermined time intervals using a Lambda 35 Spectrophotometer (Perkin Elmer, Waltham, MA, USA). Fourier transform infrared spectroscopy (FTIR) spectra of solid samples were recorded on a FTIR spectrometer (Spectrum RX1; Perkin Elmer) in the frequency range of 4,000–400 cm^{-1}. The crystalline nature of synthesized RGO was investigated by using a X'Pert Pro diffractometer (PANalytical, Almelo, the Netherlands). The XRD was operated at 45 kV with a current of 35 mA using Cu/kα radiation (λ=1.54060 Å). Thermogravimetric analysis (TGA) was performed under a nitrogen flow (50 mL/min) using a TGA/differential scanning calorimetry 1, Stare System (Mettler Toledo Inc., OH, USA). Samples were heated from room temperature to 1,000°C at 5°C/min. Ultrasonication was employed by using a Cole Parmer dip-stick sonicator (20 kHz ±5 kHz), which has a tapered microtip of 0.25 inches, with an amplitude of 40%. Zetasizer Nano ZS (Malvern Instruments, Malvern, UK) was used to analyze the hydrodynamic diameter of the particles. Samples dispersed in absolute ethanol were drop-casted on Si substrate and dried in air before subjecting to Raman and X-ray photoelectron spectroscopy (XPS) analysis. Raman spectra were acquired on an inVia Raman Microscope (Renishaw, Gloucestershire, UK) with 514 nm laser excitation source. XPS measurements were performed using a Kratos Axis Ultra (Shimadzu, Kyoto, Japan) spectrometer equipped with a monochromatized Al kα radiation and frequency of hv =1,486.6 eV. The graphene/ethanol suspension was also drop-casted on Cu grid (3 nm thick) and mica substrate for high resolution transmission electron microscopy (HRTEM), AFM, and field emission scanning electron microscopy (FESEM). HRTEM images were acquired using a Philip model (JOEL, Tokyo, Japan) operating at an accelerating voltage of 120 kV. The thickness of graphene materials was examined using a 5500 Agilent Technologies AFM System (Agilent Technologies, Santa Clara, CA, USA) using ultrasharp tips (non-contact high resonance frequency, nanosensor probe). Morphological analysis was carried out using field emission gun scanning electron microscopy Quanta SEM 400 instrument (FEI, Oregon, USA). Electrochemical studies were conducted by cyclic voltammetry (CV) measurements with a Princeton Applied Research Versastat electrochemical station. Potential range was set at −0.1 V to 0.6 V with a scan rate of 50 mV/s. Three electrode cells were used; a Ag/AgCl as the reference electrode; platinum wire as the counter electrode; and a bare and modified glassy carbon electrode (GCE) as the working electrode. Results were collected after at least 5 CV runs.

Preparation of GO

GO was produced at room temperature based on the modified Hummer's method.[39] Briefly, H_2SO_4 (95%) and H_3PO_4 (88%) were added in the ratio of 9:1 to 3 g of graphite, followed by a slow addition of 18 g of $KMnO_4$. The resulting inhomogeneous solution was allowed to stir. After 72 hours, the reaction was terminated with the addition of 400 g of ice cubes followed by 18 mL of H_2O_2 (30%). The mixture was then centrifuged at 6,000 rpm for 10 minutes. To the supernatant, 1 M HCl was added to discard the sulfate and phosphate ions followed by centrifugation at 11,500 rpm for 30 minutes. This was repeated three times followed by washing with deionized water six times. The final mixture was a viscous brown GO solution. A standard calibration curve of GO was generated by measuring the characteristic absorbance of GO at 230 nm using a UV–Vis spectrophotometer. The concentration of the prepared GO was found to be 10 mg/mL.

Preparation of GL extract

One hundred milliliters of Milli-Q water was added to 1 g of GL mushroom powder and the mixture was allowed to boil at 95°C for 3 hours. To remove the spent powder, the mixture was centrifuged at 10,000 rpm for 15 minutes. The solution was then stored at 4°C and was used directly for the reduction of GO (as mentioned in "Preparation of RGO using GL extract").

Determination of the concentration of GL extract

Concentration of the GL mushroom extract was determined using the phenol–sulfuric acid assay[40] with glucose as a reference. Briefly, 30 mL of ethanol was added to 10 mL of GL extract and stored overnight at 4°C. The crude polysaccharide precipitate was then separated by centrifugation at 10,000 rpm for 15 minutes and the clear supernatant was then subjected to vacuum drying at 40°C to obtain a solid powder. The powder was then dissolved in 1 mL of Milli-Q water and 0.1 mL was taken to determine the concentration following the method as reported by DuBois et al.[40] The concentration obtained was found to be 1 mg/mL.

Preparation of RGO using GL extract

pH adjustments were carried out on the GO solution (0.1 mg/mL) by using NaOH to obtain pH 7. Fifty milliliters of GL extract was then added to a 50 mL of GO solution and transferred to a water bath which was preheated to 85°C and allowed to react for 16 hours at a mixing rate of 120 rpm. The resulting black dispersion was then ultracentrifuged at 10,000 rpm for 20 minutes to remove the GL extract. The product was then washed three times with water to further remove the residual GL extract. The resulting black RGO dispersion was then redispersed in water.

Reusability of GL extract

The GL extract, which had been separated as described above, was reused for two more cycles to reduce the freshly prepared GO using the same reduction protocol. UV–Vis measurements were used to determine the amount of GO that was converted to RGO by determining the intensity of RGO peak at 260 nm. In each case, the amount of GO converted to RGO was calculated.

GO and RGO size analysis and solubility test

Five minutes of ultrasonication with a microtip was carried out to disperse the GO and RGO before subjecting to size distribution by dynamic light scattering (DLS). For the solubility test, RGO was dispersed in water, phosphate-buffered saline, ethanol, methanol, and acetone by ultrasonication for 5 minutes. The dispersed samples were kept at room temperature (RT) and observation was continued for 12 months.

Electrochemical measurements

For CV measurements, 1 M Na_2SO_4 was used as an electrolyte. Five microliters of GO or RGO dispersed in ethanol was dropped on a cleaned GCE and dried in an oven at 60°C for 5 minutes.

Cell lines and culture conditions

Human grade IV glioblastoma (U87MG), colon adenocarcinoma (HT-29), and normal lung fibroblast (MRC-5) cells were used in this study. HT-29 and MRC-5 cells were cultured with RPMI (Roswell Park Memorial Institute) 1640 medium (Nacalai Tesque, Kyoto, Japan) whilst U87MG cells were cultured with MEM (minimum essential medium) containing sodium pyruvate (Nacalai Tesque). The steps on propagation and maintenance of the cells were followed as described previously.[41]

Neutral red uptake assay

Cell viability of GO and RGO treatments was performed by neutral red uptake assay on U87MG, HT-29, and MRC-5 cells as described by Lim et al.[42] A total of 5×10^3 cells were seeded in 96-well plates (SPL Life Sciences, Gyeonggi, South Korea) and incubated overnight for attachment. The cells were treated with 200 µL of media containing 0.1–50 µg/mL of GO and RGO, whereas cells grown in media without any treatment were used as a negative control. Following 48 hours of incubation at 37°C, the percentage of cell viability was determined. All experiments were carried out in triplicate in three independent experiments. Absorbance readings of the plates were captured by using a microplate reader (Thermo Fisher Scientific) at 490 nm.

Statistics

Statistical analysis was performed using the Graphpad Prism (version 5) software. One-way analysis of variance was used to test for statistical significance between treated and untreated groups using Dunnett's *t*-test. Meanwhile, comparison amongst treatment groups was done by two-way analysis of variance using Bonferroni *t*-test.

Results and discussion

The reduction of GO using GL extract was monitored by time-dependent UV–Vis spectroscopy as shown in Figure 1. The strong absorption peak at 230 nm (0 hours) is a distinctive peak of GO which corresponds to π–π* transition of C=C bond, and the shoulder at 300 nm is due to n–π* transition of the C=O bonds in GO. Gradual red shifting of the 230 nm peak towards 260 nm can be seen during the reaction, suggesting the restoration of π-conjugation network of RGO after reduction. Moreover, the gradual disappearance of plasmon

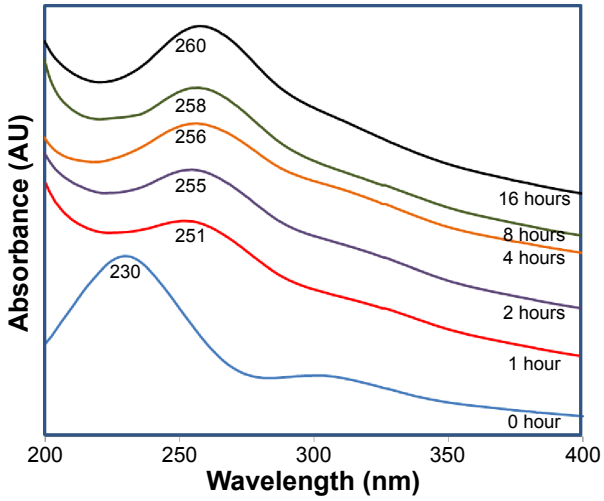

Figure 1 Ultraviolet–visible spectra of graphene oxide reduction with *Ganoderma lucidum* extract at different time intervals.

peak at 300 nm confirms the removal of oxygen groups in RGO.[3,43,44] The formation of RGO was observed within 1 hour with the red shift of a typical GO peak at 230 nm to 251 nm. Highest absorbance was observed at 16 hours, which indicates that reaction time is directly proportional to the amount of RGO formed.

Changes in the color of solution are a good indicator of GO reduction. The brown GO solution before reaction turned to a black dispersion after reaction as shown in Figure 2A, which indicates the successful conversion of GO to RGO. In order to optimize the reaction conditions, two control experiments were conducted: 1) by mixing GO and GL extract at RT; and 2) heating the GO solution without GL extract at 85°C. After 16 hours, no change in the color was observed in the GO–GL mixture that was kept at RT. However, a marginal red shift to 240 nm could be observed (Figure 2B) in the UV–Vis spectrum with a shoulder peak at around 300 nm suggesting that only an insignificant amount of GO was converted to RGO, thus confirming the need of heat for a complete reduction of GO to take place. Heat is often introduced in the reduction of GO to allow its thermal expansion and exfoliation to produce single or few-layered graphene sheets.[45] In addition, similar to conventional hot water extraction, heat is required in this reaction to further breakdown the cell walls of the mushroom and to liberate the polysaccharides[46] which have the reducing properties. However, heating of GO alone without GL extract did not convert GO to RGO, as confirmed by the absence of absorbance peak at 260 nm in the UV–Vis spectrum. The corresponding image as shown in Figure 2A illustrates that GO solution has turned to dark brown, probably due to the heat which induces darkening of the solution but does not convert GO to RGO, thus verifying the need of GL extract as a reducing agent. In comparison, reaction of GO with GL extract at 85°C produces a distinctive peak of graphene, appearing at 260 nm. Hereafter, the GO reduced by GL extract at 85°C is labeled as RGO.

To determine the capability of mushroom extract for its reusage in the reduction, GL extract after first usage was separated from the product via simple ultracentrifugation and

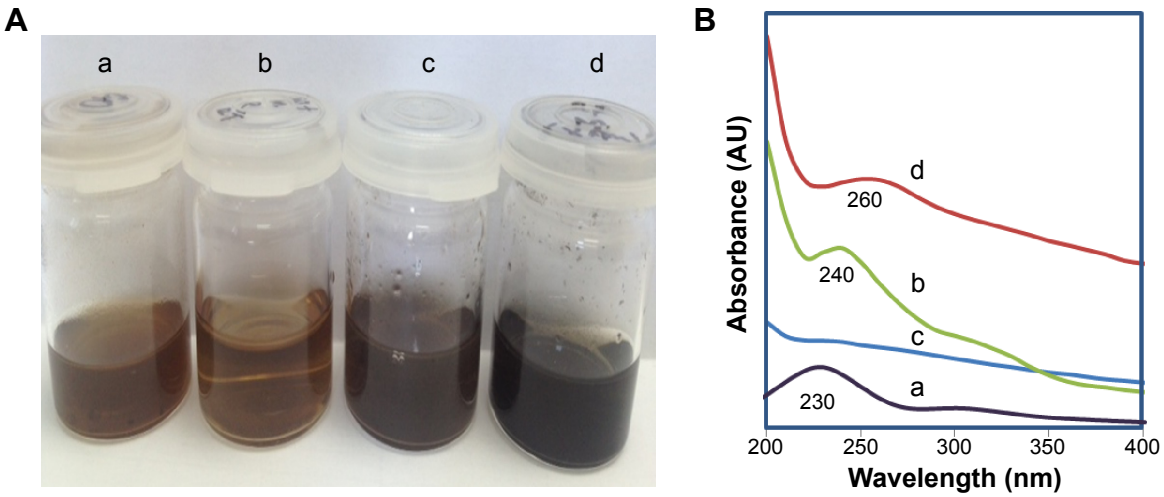

Figure 2 Preparation of RGO and the corresponding characterizations by ultraviolet-visible spectroscopy.
Notes: (**A**) Photographs of: (a) GO (0.1 mg/mL) before reaction, (b) GO GL extract at RT, (c) GO without GL extract heated at 85°C, and (d) GO GL extract heated to 85°C. (**B**) Corresponding UV–Vis spectra of reactions: (a) GO (0.1 mg/mL) before reaction, (b) GO GL extract at RT, (c) GO without GL extract heated at 85°C, and (d) GO GL extract heated to 85°C.
Abbreviations: GL, *Ganoderma lucidum*; GO, graphene oxide; RGO, reduced graphene oxide; RT, room temperature; UV–Vis, ultraviolet–visible.

Table 1 Conversion of GO to RGO with the reuse of GL extract

Cycle	Conversion (%)
First	100
Second	95
Third	75

Abbreviations: GL, *Ganoderma lucidum*; GO, graphene oxide; RGO, reduced graphene oxide.

reused to reduce the GO. By assuming a complete reduction in the first usage, about 75% conversion of GO was still observed even after the third use of GL extract as shown in Table 1. This indicates that GL extract can be reused several times without significantly losing its reducing properties, which could be lucrative for large-scale production of RGO. The conversion of GO to RGO was calculated by measuring the absorbance of RGO at 260 nm and the amount of RGO formed was determined by using a RGO standard calibration curve. In the first cycle, 5 mg of GO was found to produce 5 mg of RGO, thus showing a 100% conversion.

The formation of RGO is further confirmed by FTIR spectroscopy as shown in Figure 3A. FTIR spectra of GO shows a strong absorption peak of ν_{O-H} at 3,412 cm^{-1} due to stretching vibration and a deformation peak at 1,396 cm^{-1} due to the hydroxyl groups located on the plane of GO. Carboxyl groups at the edges of GO sheets show stretching vibration and the $\nu_{C=O}$ peak appears at 1,726 cm^{-1}. The spectra also exhibit several characteristic peaks of GO; $\nu_{C=C}$ at 1,630 cm^{-1} due to the aromatic C=C bonds; ν_{C-O} at 1,246 cm^{-1} due to epoxy C-O stretching vibration; and ν_{C-O} at 1,116 cm^{-1} due to alkoxy C-O stretching vibration.[4,12,47] Comparing with graphite (Figure 4A), the GO spectrum indicates successful oxidation with the presence of hydroxyl, epoxy, alkoxy, and carboxyl functional groups. Successful deoxygenation could be seen for RGO with the disappearance and reduced intensity of all the oxide functional groups. A broad C-O band that appears from 1,214 to 1,000 cm^{-1} even after reduction could be attributed to oxygen atoms or cyclic ether accumulated at the edges of defects in RGO. This indicates that all the oxygen groups are removed from the region adjacent to edges and only clean graphene domains are present in RGO.[2,48] It is reported that the oxygen moieties present on the edges of RGO do not affect the electronic properties of RGO.[49] The spectra of GL extract exhibit a broad band around 3,397 cm^{-1} due to the stretching of N-H and O-H groups, and a corresponding N-H bending at 1,639.5 cm^{-1}. Other characteristic peaks of GL extract are at 2,930 cm^{-1} and at 2,884.9 cm^{-1} due to the asymmetric stretching of CH_3 and symmetric stretching of CH_2, respectively. The sharp peaks at 1,074.4 cm^{-1} and at 1,046.5 cm^{-1} are due to C-O stretching and bending of C-OH in the polysaccharide.[50,51] The absence of these characteristic peaks in RGO confirms the complete removal of GL extract after the reaction.

XRD analysis (Figure 3B) is a good tool to estimate the interlayer spacing between the graphitic layers and the crystalline properties, as well as to determine the completion of reaction. Graphite exhibits a strong basal reflection (002) peak at 2θ=26.6° with an interlayer distance (d-spacing) of approximately 0.33 nm. This intense crystalline peak is a characteristic peak of hexagonal pristine graphite. The disappearance of this peak in GO confirms the complete oxidation of graphite. Upon oxidation, the diffraction peak (001) of GO appears at a lower angle (2θ=9.2°) with a d-spacing of 0.96 nm. The larger interlayer spacing after

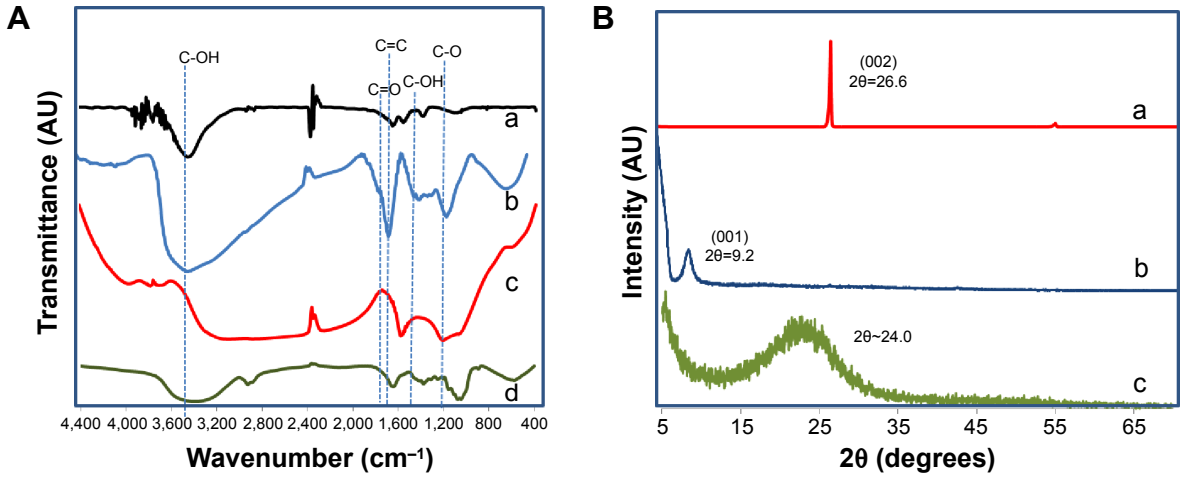

Figure 3 Characterizations of RGO by FTIR and XRD.
Notes: (**A**) FTIR spectra of (a) graphite, (b) GO, (c) RGO, and (d) GL extract; (**B**) XRD patterns of (a) graphite, (b) GO, and (c) RGO.
Abbreviations: FTIR, Fourier transform infrared spectroscopy; GO, graphene oxide; RGO, reduced graphene oxide; GL, *Ganoderma lucidum*; XRD, X-ray diffraction.

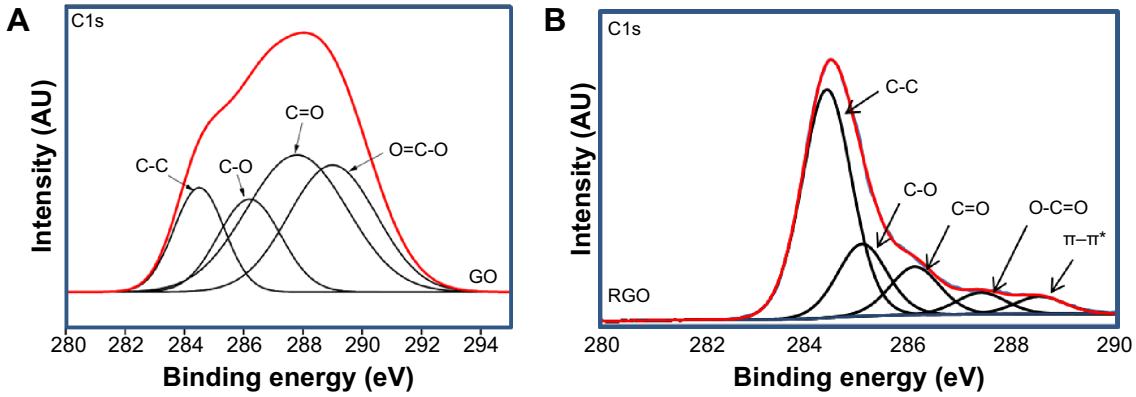

Figure 4 XPS spectra of C1s.
Notes: (**A**) GO and (**B**) RGO.
Abbreviations: GO, graphene oxide; RGO, reduced graphene oxide; XPS, X-ray photoelectron spectroscopy.

oxidation is due to the intercalation of oxide functional groups on both sides of GO sheets. In addition, structural defects (sp^3 bonding) generated on the originally flat graphite sheets contribute to atomic-scale roughness and thus a larger d-spacing of GO.[52] After reduction, the distinctive GO peak of RGO disappears, indicating a complete reduction as well as exfoliation of the layered RGO sheets.[22,53] A broad peak has been observed for RGO, starting from $2\theta=15°$ to $2\theta=30°$, with the peak centered at $2\theta=24°$, and a d-spacing of 0.37 nm. The appearance of this peak at 24.0° is due to restoration of van der Waals' interaction between the carbon frameworks on the graphene sheets upon reduction. The presence of a broad peak indicates the loss of long range order in the graphene sheets, the graphene sheets are stacked with few-layers.[17,47,54,55] In addition, the significant reduction in the interlayer spacing of RGO as compared to GO suggests the removal of oxygen groups and water molecules from the interlayer of graphene sheets in RGO. However, a difference in the interlayer distance of approximately 0.04 nm between the pristine graphite and RGO is observed. This is probably due to the fact that it is impossible to revive the original π–π stacking between the graphene sheets after the extreme intercalation of oxygenous groups into the graphite during the chemical oxidation process. The GO sheets had probably crumpled during the exfoliation stage and remained in that position even after reduction.[56]

The formation of RGO was further confirmed by XPS analysis. The C1s of GO as shown in Figure 4A demonstrates the highest intensity at the binding energy of 287.8 eV, which belongs to carbonyl functional groups. Other peaks at 284.8, 286.3, and 289.1 eV correspond to C=C/C-C in aromatic rings; C-O in hydroxyl and epoxy groups; and O-C=O in carboxyl groups, respectively.[12,17,57] After reduction, the peak intensity for all the oxygen species decreased dramatically, suggesting the effective removal of oxygen-containing groups in RGO. In addition, a sharp increase in the C=C/C-C peak at 284.4 eV and the appearance of a π–π* peak at 288.5 eV indicate the restoration of sp^2 carbon network.[58] C/O molar ratio calculated from the peak areas shows a very high content of oxygen species in GO (1:13.6), whereas in RGO, the molar ratio was found to be only 1:2.16, again confirming the successful reduction of GO.

Figure 5 shows the FESEM images of GO and RGO. It could be observed that GO (Figure 5A) has continuous and smooth wave-like sheets, whereas a flake-like morphology could be noted in RGO (Figure 5B), which forms a disordered solid with the individual sheets closely stacked. With the removal of oxygen groups from the basal plane as well as from the edges of RGO, the graphene sheets were then allowed to closely associate and stack via van der Waals' interactions. This finding is in good agreement with the results of XRD obtained for RGO, where the d-spacing or interlayer distance is smaller than GO, permitting the stacking of RGO flakes. The RGO flakes lie flat on top of each other, suggesting the possibility of good electrical contact between them.[59] The microstructure of GO and RGO was further investigated by HRTEM. It could be seen that GO has a wavy structure with few well-defined layers of stacking at the edges (Figure 5C). The observed stacking could be due to strong hydrogen bonding interaction between the GO layers or with water molecules.[60] As for RGO, thin veil-like sheets were observed with scrolling and wrinkles, which confirms that reduction of GO has taken place. It was reported that scrolling is caused by the presence of isolated epoxy and hydroxyl groups, whereas the wrinkles are due to the removal of strain on the C-C bond in the epoxy groups

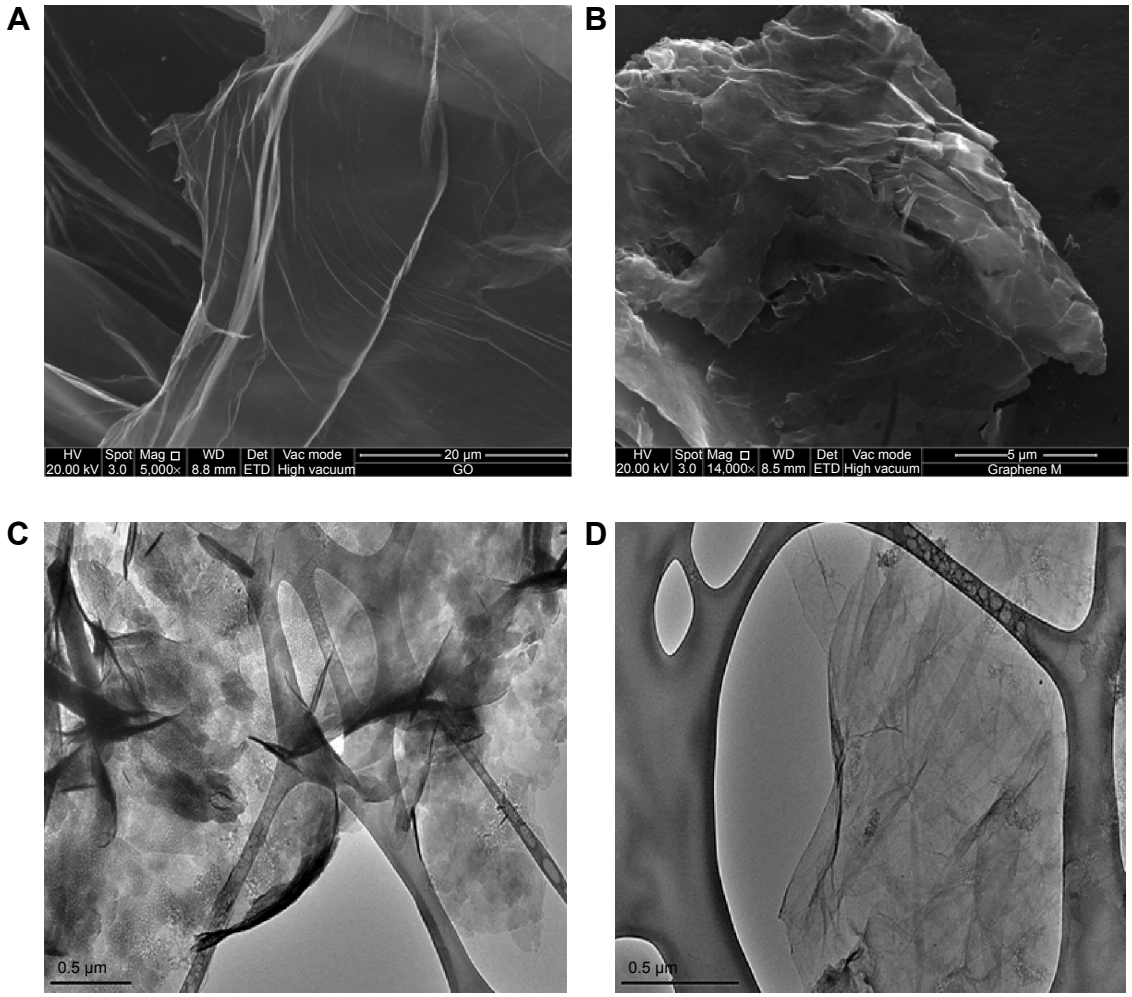

Figure 5 Characterization of RGO by FESEM and HRTEM.
Notes: FESEM images of (**A**) GO and (**B**) RGO, and HRTEM images of (**C**) GO and (**D**) RGO.
Abbreviations: FESEM, field emission scanning electron microscopy; GO, graphene oxide; HRTEM, high resolution transmission electron microscopy; RGO, reduced graphene oxide.

which was created during the formation of three-membered epoxide rings in GO.[61] In addition, RGO appeared transparent, which is similar to the graphene produced from electrolytic exfoliation of graphite as reported by Wang et al.[62] The lateral dimension of RGO in both FESEM and HRTEM was approximately 500 nm.

To further confirm the reduction of GO, Raman spectroscopy was used to investigate the nature of layering and defects on the graphitic sheets. Generally, the Raman spectra exhibit four main featured peaks: D, G, 2D, and D plus G bands. D band is attributed to the graphene sheet edges and defects, activated by the presence of disorder, whereas the G band originates from the first-order scattering of E2g phonon of sp^2 carbon atoms. The Raman spectra of graphite (Figure 6Aa) displays a sharp G band at 1,582 cm^{-1} due to in-phase vibration of the graphite lattice and a weak D band at 1,370 cm^{-1} indicating low degree of defects that are mostly due to the sheet edges. In comparison, GO exhibits a prominent G band which is blue-shifted to 1,586 cm^{-1} signifying the presence of isolated double bonds which resonate at higher frequencies than that of graphite. The intensity of the D band at 1,352 cm^{-1} was also increased which could be attributed to the decrease in size of in-plane sp^2 domains compared to graphite.[12,17,22,52] For RGO, the G band is broadened, shifted to 1,611 cm^{-1}, and moved closer to the G band of graphite, which is attributed to graphitic self-healing and successful reduction,[63] as the removal of oxygen groups allows the RGO to associate and restack. The D band of RGO becomes more prominent and remains almost at the same position as GO, ie, at 1,351 cm^{-1}.

The intensity ratio of D to G is a good indicator of the degree of distortion in the graphitic sheets. As expected, the intensity ratio of RGO has dramatically increased to 0.99 as compared to GO (0.94) and graphite (0.07). A higher intensity

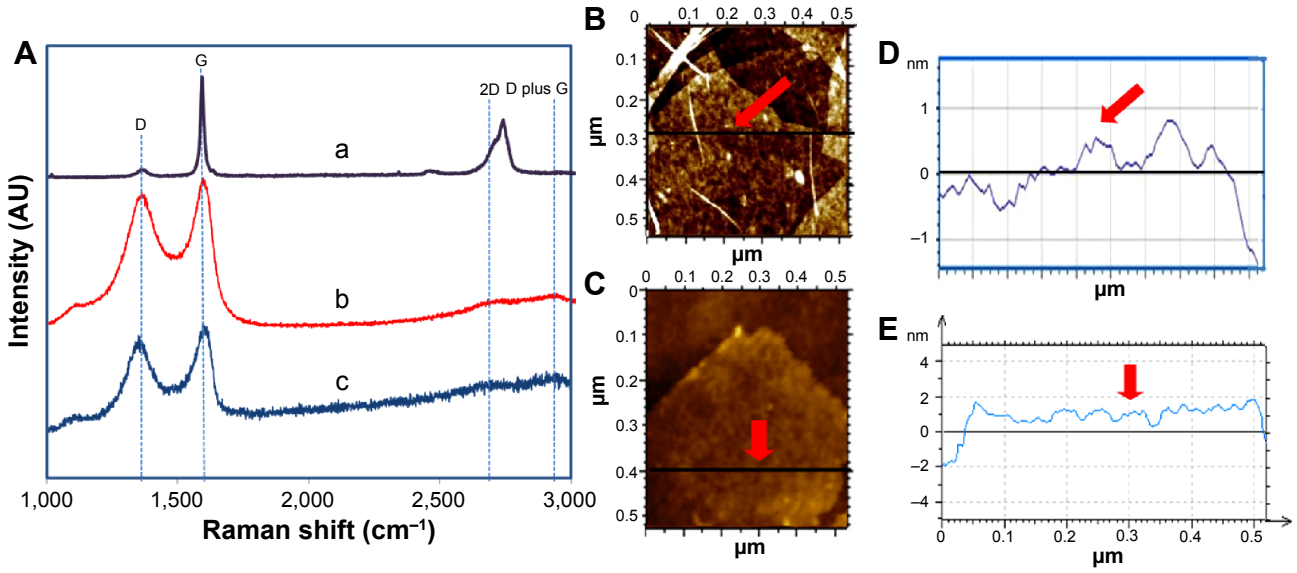

Figure 6 Raman spectroscopy analysis and AFM images with its corresponding height profiles.
Notes: (**A**) Raman spectra of (a) graphite, (b) GO, and (c) RGO. AFM images of (**B**) GO and (**C**) RGO with respective thickness measurements were taken along the cross-section, as indicated by a line and a red arrow for (**D**) GO and (**E**) RGO.
Abbreviations: AFM, atomic force microscopy; GO, graphene oxide; RGO, reduced graphene oxide.

ratio as seen in GO compared to graphite is due to the introduction of defects after oxidation of graphite, whereas the highest intensity ratio seen in RGO indicates disorder on the graphene sheets after reduction and an increase in the number of sp^2 domains. It is suggested that the reduction of GO causes fragmentation and yields smaller RGO graphitic domains with different sizes.[64,65]

The 2D band represents the symmetry-allowed overtone of the G band. The shift, shape, and width of the 2D peak are sensitive to stacking order of the graphene sheets along the C-axis and the number of graphene layers, in which single-layered graphene has a single sharp Lorentzian peak below 2,700 cm^{-1}. Multiple layered sheets have broader and upshifted 2D peaks.[3,47,52,66] The broad 2D band of graphite from 2,627 to 2,776 cm^{-1} indicates the presence of multiple layered graphite sheets, whereas the 2D band of GO at 2,700 cm^{-1} indicates a single layered sheet. After reduction, this peak has marginally broadened and shifted to 2,769 cm^{-1} suggesting the presence of three-layered graphene sheets.[67] The cooperation between D and G peaks gives the D plus G combination band which indicates the presence of highly disordered and randomly arranged graphene sheets.[3,4] The D plus G band is observed for GO at 2,690 cm^{-1} and a slightly broader band is observed for RGO at 2,692 cm^{-1}, indicating the presence of more random arrangement in RGO. The absence of these peaks in graphite shows that it exists as a continuous long sheet.

GO and RGO were then subjected to AFM to determine their respective topography as well as thickness. The cross-section from AFM analysis shows that the maximum thickness of GO is approximately 1 nm, which is in compliance with the d-spacing of GO, ie, 0.96 nm as determined by XRD. After reduction, the RGO's thickness is approximately 1–2 nm. The thickness obtained is similar to those produced from hydrazine reduced GO[68,69] and hydrothermally reduced GO.[61] Based on the XRD analysis of RGO with 0.37 nm d-spacing, it could be estimated that RGO is few-layered (3–5 layers), similar to the observation from Raman analysis.

The particle size distribution of aqueous dispersion of GO and RGO was determined by DLS analysis. Although DLS is more suitable for spherical particles rather than for planar sheets like graphene, it serves to indicate whether uniformly sized dispersion of graphene was produced, besides demonstrating the changes in the size of GO and RGO. As shown in Figure 7, the average size of GO and RGO was 313 nm and 181 nm, respectively. In GO, the peak appearing after 1,000 nm could be due to the presence of remnants from the reaction of graphite oxidation. Also, the presence of undisrupted long continuous sheets in the GO results in larger size. RGO, however, shows a uniform size distribution with sizes generally at least two-times smaller than GO. This concludes that there is a loss of long-range graphitic order in RGO and corroborates the observation of a D plus G peak in the XRD spectra. The smaller sized RGO observed, as compared to other reported methods,[52,70] could be mainly due to the method of synthesis employed and due to the effect of 5 minutes of ultrasonication. Reduction of GO with *E. coli*[12] followed by sonication yields graphene

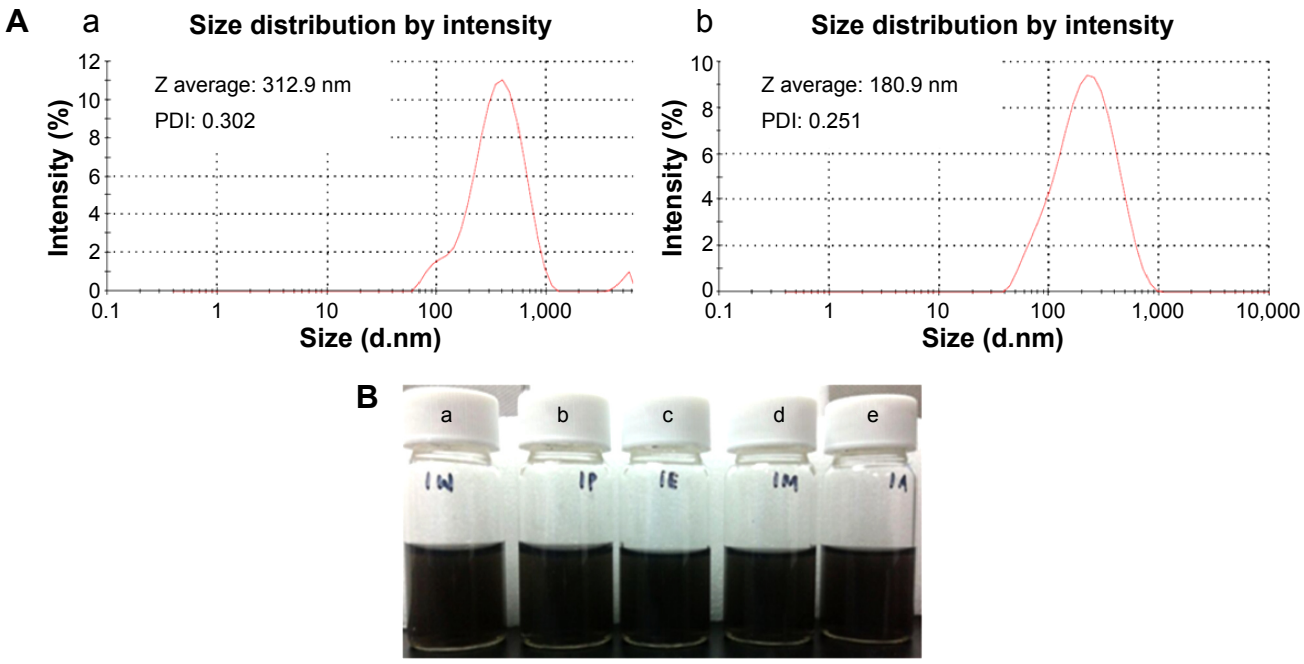

Figure 7 DLS characterization and photograph of RGO dispersion in different solvents.
Notes: (**A**) Size distribution analysis on (a) GO and (b) RGO with respective PDI and size. (**B**) Solubility of RGO in (a) water, (b) PBS buffer, (c) ethanol, (d) methanol, and (e) acetone.
Abbreviations: PBS, phosphate-buffered saline; GO, graphene oxide; PDI, polydispersity index; RGO, reduced graphene oxide; Z, size; DLS, dynamic light scattering.

with the size of 702 nm, which is almost seven-times larger than the size of RGO obtained through our strategy. Generally, ultrasonication breaks the RGO nanosheets to smaller fragments; a similar observation was also noted in GO.[71] In addition, ultrasonication of RGO results in better dispersion in water. A solubility test (Figure 7) showed that RGO is stable in the tested solvents for up to 12 months, without any visible aggregation or sedimentation. It is reported that ultrasonic treatment induces cavitation near surfaces of RGO sheets, which inhibits the aggregation of RGO by weakening its van der Waals' interactions and, thus, enhances the formation of stable RGO dispersion.[58] Besides, the presence of oxygen groups at the edges of defects in RGO sheets, as observed in FTIR spectra, could have contributed to the better stability and solubility of the produced RGO.

Thermal stability of graphite, GO, and RGO was analyzed using TGA (Figure 8A). GO exhibits much more prominent weight loss as compared to graphite and RGO due to the presence of a larger amount of oxygen groups. Below 100°C, GO has the highest weight loss of about 14.5%, owing to the removal of water molecules, whereas no weight loss was observed for graphite; but a weight loss of 5% could be observed in the case of RGO, which may be due to the removal of adsorbed water molecules. From 100°C to 200°C, GO again had the highest weight loss of about 25% due to the removal of labile oxygen functional groups: CO, CO_2, and possibly remaining water molecules. Weight loss in this region was not observed in graphite, but RGO had a weight loss of approximately 14%, indicating the probable presence of residual GO or water molecules. The highest weight loss was observed from 200°C to 400°C for all three graphitic materials, ie, GO (21%), graphite (1%), and RGO (9%), which is due to bulk pyrolysis of the carbon skeleton. The highest weight loss as seen in GO for this region is due to the complete removal of residual oxygen functional groups. RGO displays better thermal stability as compared to GO due to the comparatively fewer oxygen groups and restoration of weak van der Waals' forces between the graphene layers.[54]

To ascertain whether the followed synthesis method affected RGO's electrochemical characteristics, a CV measurement was conducted (Figure 8B). All CV curves were recorded after several cycles of CV and when they became stable. CV of GO/GCE demonstrated almost no electrical potential, with CV curves overlapping those of bare GCE. After reduction, far superior electrical potential was observed for RGO/GCE, with a higher value of current response and CV area. This is largely contributed by an increase in electron transfer in the RGO layer and electronic transition between the RGO layers. The voltammogram for GO showed obvious oxygen and hydrogen evolution peak (indicated by a red arrow in Figure 8Bb), whereas the absence of this

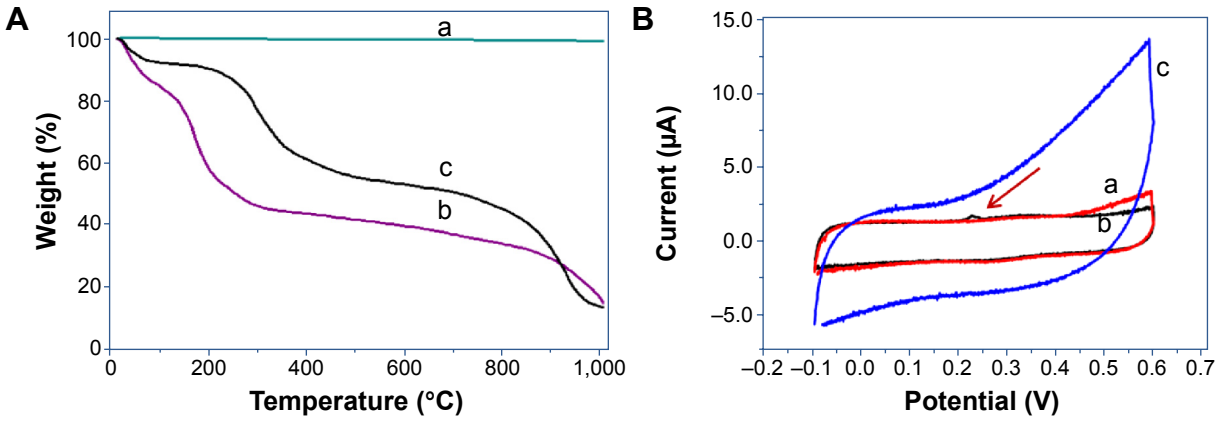

Figure 8 Thermal and electrochemical analysis of RGO using TGA and cyclic voltammetry.
Notes: (**A**) TGA curves of (a) graphite, (b) GO, and (c) RGO. (**B**) Cyclic voltammogram obtained for (a) GCE, (b) GO/GCE, and (c) RGO/GCE. The red arrow indicates oxygen and hydrogen evolution peak.
Abbreviations: GCE, glassy carbon electrode; GO, graphene oxide; RGO, reduced graphene oxide; TGA, thermogravimetric analysis.

peak in RGO with typical rectangular curve indicates good charge propagation with electrodes and ideal capacitive behavior.[54,72]

Previous reports demonstrated that graphene exhibited significant biocompatibility towards numerous cells such as L929 mouse fibroblast cells and A549 human lung cancer cells, and it possessed toxicity only towards a few specific cells.[47,73] The variation in the cytotoxicity profile is suggested to be mainly due to the difference in the synthesis methods (graphene reduced from GO prepared by modified Hummers method versus graphene from heat treatment of graphite or from unzipping of CNTs).[74,75] Hence, for comparison in parallel with GO, the synthesized RGO was subjected to cytotoxicity analysis on two cancer cells (ie, colon [HT-29] and brain [U87MG] cancer cells) to determine the presence of specific cancer type selectivity, as well as on normal cells (MRC-5) to ascertain whether the synthesized graphene material is suitable, especially for anticancer drug-delivery purposes without causing damage to the normal cells.

Based on the fact that viable cells incorporate and bind more dye as compared to damaged or dead cells,[76] the dose-dependent cytotoxicity of GO and RGO can be determined by neutral red uptake assay. Untreated cells were calculated as having a cell viability of 100%. Both GO and RGO showed no significant toxicity towards HT-29 cells as shown in Figure 9A. Over 90% cell confluence was observed at the highest concentration (50 μg/mL), even for GO. This is, however, in accordance with previous findings,[77] where more than 87% HT-29 cell viability was observed for graphene. A similar finding was also observed for other types of cancer cells such as HeLa cancer cells,[78] where cell viability of 90% was observed for GO at 40 μg/mL. Miao et al[79] also observed about 87% cell viability of GO towards SCC7 cells.

However, a different cytotoxicity pattern was seen in U87MG cells as shown in Figure 9B. A decrease in cell viability was observed for GO starting from 10 μg/mL when compared to untreated cells. GO has been largely reported to cause plasma membrane damage and oxidative stress, and thus antiproliferative distress to the cells.[80] On the other hand, RGO was found to be biocompatible with almost 100% cell confluence even at the highest concentration (50 μg/mL). By comparing GO with RGO, a significant difference in cell viability was observed starting from the concentration of 25 μg/mL ($P<0.01$). A previous study by Jaworski et al[81] showed that graphene demonstrated cytotoxicity toward U87MG cells, even at a lower concentration of 20 μg/mL. At 100 μg/mL, they observed only 54% cell survival, whereas the RGO obtained through our strategy is exceedingly biocompatible towards brain cancer cells as compared to other reported graphene derivatives.

GO (Figure 9C) showed obvious toxicity towards MRC-5 as compared to the untreated cells, even from concentrations as low as 5 μg/mL. A previous investigation by Wang et al[82] supports this observation, where GO was found to induce cytotoxicity, genotoxicity, and oxidative stress to MRC-5 cells. In contrast, RGO showed no cytotoxicity towards normal cell lines with the cell viability above 90%, even at 50 μg/mL. Similar findings were observed only on functionalized graphenes such as carboxyl-modified graphene, where the cell viability was about 100% when tested against normal Vero cells.[74] It was reported that pluronic-modified graphene was also observed to be similar due to the formation of stable graphene dispersion.[83] This roughly proves that covalent or noncovalent functionalization was necessary in order to create a stable and nontoxic graphene.

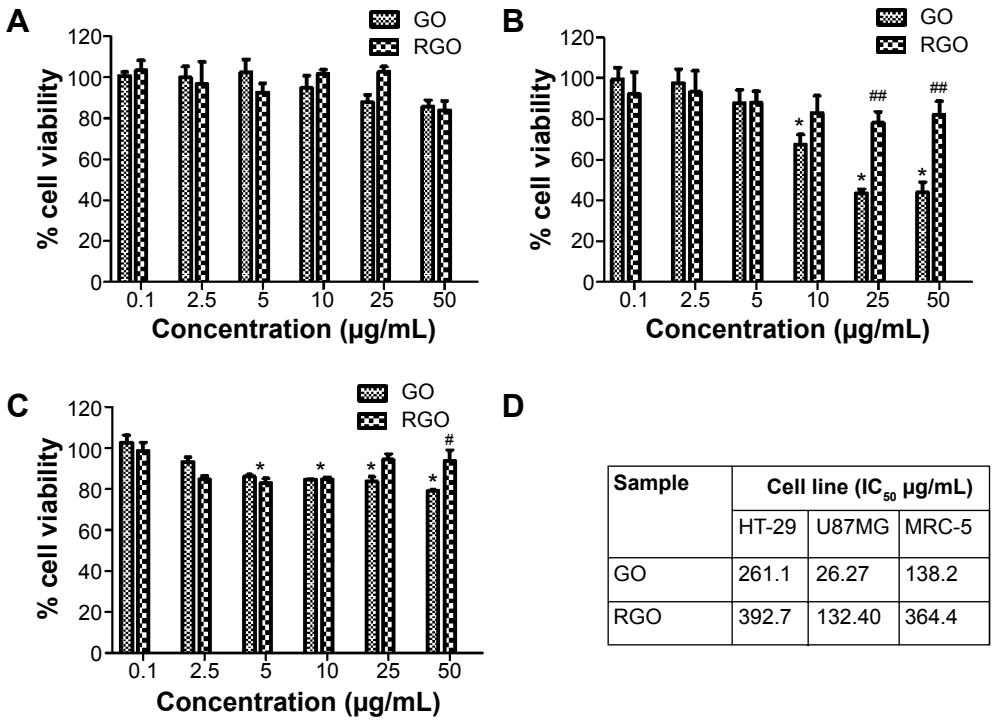

Sample	Cell line (IC_{50} μg/mL)		
	HT-29	U87MG	MRC-5
GO	261.1	26.27	138.2
RGO	392.7	132.40	364.4

Figure 9 Effect of GO and RGO on cell viability of cancer and normal cells.
Notes: The cell viability (%) on (**A**) HT-29, (**B**) U87MG, and (**C**) MRC-5 cells, and (**D**) overall IC_{50} values of GO and RGO treatments for 48 hours generated by neutral red uptake assay. Bars represent mean ± standard error of the mean of triplicates in three independent experiments (n=9). *Significant difference when treated groups were compared with untreated ($P<0.001$) using one-way ANOVA with Dunnett's *t*-test. # and ## indicate significant difference when GO was compared to RGO, with $P<0.5$ and $P<0.01$, respectively, using two-way ANOVA with Bonferroni *t*-test.
Abbreviations: ANOVA, analysis of variance; GO, graphene oxide; IC_{50}, half maximal inhibitory concentration; RGO, reduced graphene oxide.

Graphpad Prism software was used to estimate the half maximal inhibitory concentration (IC_{50}) values of GO and RGO as shown in Figure 9D. GO was found to be toxic, especially towards U87MG cells, with IC_{50} at a very low concentration of 26.27 μg/mL. As discussed earlier, this was due to the presence of oxygen functional groups in GO, which consequently lead to oxidative stress in cells and result in poor cell survival.[80] RGO showed better cell survival compared to GO for all the three cells, with IC_{50} values beyond 50 μg/mL and up to 390 μg/mL. Since the cell viability assay was conducted only up to a concentration of 50 μg/mL, the concentration values in Figure 9D only serve as an estimation generated by the software. Nevertheless, based on the current findings, our mushroom synthesized RGO, without the need of any functionalization, shows good aqueous stability and is equally biocompatible compared to the functionalized ones. Although our RGO does not possess any selectivity against the two cancer cells and normal cells tested, this feature is still of great value for the synthesized RGO to be a tool for protein/gene transfection, as well as a drug-delivery vehicle for cancer treatment, such as by conjugation of an anticancer drug.

Conclusion

An over the counter, commercial-grade mushroom powder was used to effectively reduce GO to RGO with a reaction time of just 1 hour. This environmentally friendly method avoids the use of chemicals and significantly reduces waste, with the advantage of reusability of the extract as a reducing agent. The obtained RGO was readily dispersible in water and was reasonably small, with a thickness of 1–2 nm and a 181–500 nm lateral dimension. The RGO obtained through this strategy is small as compared to other reported green-synthesis methods. In addition, solubility tests using various solvents showed that RGO is stable up to a tested period of 1 year. The employed synthetic route also did not affect its electrical conductivity. While functionalization of graphene is imperative to reduce its cytotoxicity, the current mushroom-extract-reduced RGO was found to be biocompatible even without any additional functionalization. RGO has not shown any antiproliferative effects towards colon and brain cancer or towards normal cell lines. However, substantial work remains in elucidating this exceedingly good biocompatibility, especially in exploring RGO's intracellular event. The large availability of this mushroom in Asian countries, coupled with ease of preparation, makes this

synthetic route lucrative for upscale production. Since there are no toxic chemicals involved or byproducts generated, and it is highly biocompatible towards cells, the produced RGO is suitable for biomedical applications especially in drug-delivery systems, bioimaging, and in biosensing.

Acknowledgments

The authors would like to thank Ministry of Higher Education (MOHE), Malaysia for the funding support through FRGS grant (F0018.5402) and the High Impact Research Grant (UM.C/625/1/HIR/MOHE/05).

Disclosure

The authors report no conflicts of interest in this work.

References

1. Kuila T, Bose S, Mishra AK, Khanra P, Kim NH, Lee JH. Chemical functionalization of graphene and its applications. *Prog Mater Sci.* 2012;57(7):1061–1105.
2. Singh V, Joung D, Zhai L, Das S, Khondaker SI, Seal S. Graphene based materials: Past, present and future. *Prog Mater Sci.* 2011; 56(8):1178–1271.
3. Liu K, Zhang JJ, Cheng FF, Zheng TT, Wang C, Zhu JJ. Green and facile synthesis of highly biocompatible graphene nanosheets and its application for cellular imaging and drug delivery. *J Mater Chem.* 2011;21:12034–12040.
4. An J, Gou Y, Yang C, Hu F, Wang C. Synthesis of a biocompatible gelatin functionalized graphene nanosheets and its application for drug delivery. *Mater Sci Eng C Mater Biol Appl.* 2013;33(5): 2827–2837.
5. Xu LQ, Wang L, Zhang B, et al. Functionalization of reduced graphene oxide nanosheets via stacking interactions with the fluorescent and water-soluble perylene bisimide-containing polymers. *Polymer.* 2011;52(11):2376–2383.
6. Novoselov KS, Geim AK, Morozov SV, et al. Electric field effect in atomically thin carbon films. *Science.* 2004;306(5696):666–669.
7. Berger C, Song Z, Li T, et al. Ultrathin epitaxial graphite: 2D electron gas properties and a route toward graphene-based nanoelectronics. *J Phys Chem B.* 2004;108(52):19912–19916.
8. Lee S, Lee K, Zhong Z. Wafer scale homogeneous bilayer graphene films by chemical vapor deposition. *Nano Lett.* 2010;10(11):4702–4707.
9. Kosynkin DV, Higginbotham AL, Sinitskii A, Lomeda JR, Dimiev A, Price BK, et al. Longitudinal unzipping of carbon nanotubes to form graphene nanoribbons. *Nature.* 2009;458(7240):872–876.
10. Stankovich S, Dikin DA, Piner RD, et al. Synthesis of graphene-based nanosheets via chemical reduction of exfoliated graphite oxide. *Carbon.* 2007;45(7):1558–1565.
11. Zhu P, Shen M, Xiao S, Zhang D. Experimental study on the reducibility of graphene oxide by hydrazine hydrate. *Physica B Condens Matter.* 2011;406(3):498–502.
12. Gurunathan S, Han JW, Eppakayala V, Kim JH. Microbial reduction of graphene oxide by Escherichia coli: a green chemistry approach. *Colloids Surf B Biointerfaces.* 2013;102:772–777.
13. Furst A, Berlo RC, Hooton S. Hydrazine as a reducing agent for organic compounds (catalytic hydrazine reductions). *Chem Rev*. 1965;65(1):51–68.
14. Tung VC, Allen MJ, Yang Y, Kaner RB. High-throughput solution processing of large-scale graphene. *Nat Nanotechnol.* 2009;4(1):25–29.
15. Fernández-Merino MJ, Guardia L, Paredes JI, et al. Vitamin C is an ideal substitute for hydrazine in the reduction of graphene oxide suspensions. *J Phys Chem C.* 2010;114(14):6426–6432.
16. Wang G, Yang J, Park J, et al. Facile synthesis and characterization of graphene nanosheets. *J Phys Chem C*. 2008;112(22):8192–8195.
17. Perera SD, Mariano RG, Nijem N, Chabal Y, Ferraris JP, Balkus KJ Jr. Alkaline deoxygenated graphene oxide for supercapacitor applications: An effective green alternative for chemically reduced graphene. *J Power Sources.* 2012;215:1–10.
18. Park JH, Mitchel WC, Smith HE, Grazulis L, Eyink KG. Studies of interfacial layers between 4H-SiC (0 0 0 1) and graphene. *Carbon.* 2010;48(5): 1670–1673.
19. Fan ZJ, Kai W, Yan J, et al. Facile synthesis of graphene nanosheets via Fe reduction of exfoliated graphite oxide. *ACS Nano.* 2011;5(1): 191–198.
20. Zhang J, Yang H, Shen G, Cheng P, Zhang J, Guo S. Reduction of graphene oxide via L-ascorbic acid. *Chem Commun (Camb)*. 2010;46(7): 1112–1114.
21. Liu Z, Robinson JT, Sun X, Dai H. PEGylated nanographene oxide for delivery of water-insoluble cancer drugs. *J Am Chem Soc*. 2008; 130(33):10876–10877.
22. Zhu C, Guo S, Fang Y, Dong S. Reducing sugar: new functional molecules for the green synthesis of graphene nanosheets. *ACS Nano*. 2010; 4(4):2429–2437.
23. Liu J, Fu S, Yuan B, Li Y, Deng Z. Toward a universal "adhesive nanosheet" for the assembly of multiple nanoparticles based on a protein-induced reduction/decoration of graphene oxide. *J Am Chem Soc.* 2010; 132(21):7279–7281.
24. Wang Y, Shi Z, Yin J. Facile synthesis of soluble graphene via a green reduction of graphene oxide in tea solution and its biocomposites. *ACS Appl Mater Interfaces.* 2011;3(4):1127–1133.
25. Akhavan O, Kalaee M, Alavi ZS, Ghiasi SMA, Esfandiar A. Increasing the antioxidant activity of green tea polyphenols in the presence of iron for the reduction of graphene oxide. *Carbon.* 2012;50(8):3015–3025.
26. Kim YK, Kim MH, Min DH. Biocompatible reduced graphene oxide prepared by using dextran as a multifunctional reducing agent. *Chem Commun*. 2011;47:3195–3197.
27. Salas EC, Sun Z, Lüttge A, Tour JM. Reduction of graphene oxide via bacterial respiration. *ACS Nano.* 2010;4(8):4852–4856.
28. Chen T, Pan L, Yu K, Sun Z. Microwave-assisted synthesis of reduced graphene oxide-carbon nanotube composites as negative electrode materials for lithium ion batteries. *Solid State Ionics.* 2012;229: 9–13.
29. Paterson RR. Ganoderma – a therapeutic fungal biofactory. *Phytochemistry.* 2006;67(18):1985–2001.
30. Saltarelli R, Ceccaroli P, Iotti M, et al. Biochemical characterisation and antioxidant activity of mycelium of *Ganoderma lucidum* from Central Italy. *Food Chem*. 2009;116(1):143–151.
31. Kozarski M, Klaus A, Nikšić M, et al. Antioxidative activities and chemical characterization of polysaccharide extracts from the widely used mushrooms *Ganoderma applanatum*, *Ganoderma lucidum*, *Lentinus edodes* and *Trametes versicolor*. *J Food Compost Anal.* 2012; 26(1–2):144–153.
32. Shi M, Zhang Z, Yang Y. Antioxidant and immunoregulatory activity of *Ganoderma lucidum* polysaccharide (GLP). *Carbohydr Polym*. 2013; 95(1):200–206.
33. Kozarski M, Klaus A, Niksic M, Jakovljevic D, Helsper JPFG, Van Griensven LJLD. Antioxidative and immunomodulating activities of polysaccharide extracts of the medicinal mushrooms *Agaricus bisporus*, *Agaricus brasiliensis*, *Ganoderma lucidum* and *Phellinus linteus*. *Food Chem.* 2011;129(4):1667–1675.
34. Wu DT, Xie J, Hu DJ, Zhao J, Li SP. Characterizations of polysaccharides from *Ganoderma* spp. using saccharide mapping. *Carbohydr Polym.* 2013;97(2):398–405.
35. Nie S, Zheng H, Li W, Xie M. Current development of polysaccharides from *Ganoderma*: isolation, structure and bioactivities. *Bioactive Carbohydrates and Dietary Fibre.* 2013;1(1):10–20.
36. Zhao L, Dong Y, Chen G, Hu Q. Extraction, purification, characterization and antitumor activity of polysaccharides from *Ganoderma lucidum*. *Carbohydr Polym.* 2010;80(3):783–789.

37. Chen Y, Xie MY, Nie SP, Li C, Wang YX. Purification, composition analysis and antioxidant activity of a polysaccharide from the fruiting bodies of *Ganoderma atrum*. *Food Chem*. 2008;107(1):231–241.
38. Gurunathan S, Han J, Park JH, Kim JH. An in vitro evaluation of graphene oxide reduced by *Ganoderma* spp. in human breast cancer cells (MDA-MB-231). *Int J Nanomedicine.* 2014;9:1783–1797.
39. Huang NM, Lim HN, Chia CH, Yarmo MA, Muhamad MR. Simple room-temperature preparation of high-yield large-area graphene oxide. *Int J Nanomedicine.* 2011;6:3443–3448.
40. DuBois M, Gilles KA, Hamilton JK, Rebers PA, Smith F. Colorimetric method for determination of sugars and related substances. *Anal Chem*. 1956;28(3):350–356.
41. Lim SW, Ting KN, Bradshaw TD, et al. *Acalypha wilkesiana* extracts induce apoptosis by causing single strand and double strand DNA breaks. *J Ethnopharmacol.* 2011;138(2):616–623.
42. Lim SW, Loh HS, Ting KN, Bradshaw TD, Zeenathul NA. Acalypha wilkesiana ethyl acetate extract enhances the in vitro cytotoxic effects of α-tocopherol in human brain and lung cancer cells. *Int J Biosci Biochem Bioinforma*. 2013;3(4):335–340.
43. Han Y, Luo Z, Yuwen L, Tian J, Zhu X, Wang L. Synthesis of silver nanoparticles on reduced graphene oxide under microwave irradiation with starch as an ideal reductant and stabilizer. *Appl Surf Sci.* 2013; 266:188–193.
44. Zhou Y, Bao Q, Tang LAL, Zhong Y, Loh KP. Hydrothermal dehydration for the "green" reduction of exfoliated graphene oxide to graphene and demonstration of tunable optical limiting properties. *Chem Mater.* 2009; 21(13):2950–2956.
45. McAllister MJ, Li JL, Adamson DH, et al. Single sheet functionalized graphene by oxidation and thermal expansion of graphite. *Chem Mater*. 2007;19(18):4396–4404.
46. Huang SQ, Li JW, Wang Z, Pan HX, Chen JX, Ning ZX. Optimization of alkaline extraction of polysaccharides from Ganoderma lucidum and their effect on immune function in mice. *Molecules.* 2010; 15(5):3694–3708.
47. Wojtoniszak M, Chen X, Kalenczuk RJ, et al. Synthesis, dispersion, and cytocompatibility of graphene oxide and reduced graphene oxide. *Colloids Surf B Biointerfaces.* 2012;89:79–85.
48. Acik M, Lee G, Mattevi C, Chhowalla M, Cho K, Chabal YJ. Unusual infrared-absorption mechanism in thermally reduced graphene oxide. *Nat Mater.* 2010;9(10):840–845.
49. Si Y, Samulski ET. Synthesis of water soluble graphene. *Nano Lett.* 2008;8(6):1679–1682.
50. Wang X, Chen X, Qi Z, Liu X, Li W, Wang S. A study of *Ganoderma lucidum* spores by FTIR microspectroscopy. *Spectrochim Acta A Mol Biomol Spectrosc.* 2012;91:285–289.
51. Chen X, Liu X, Sheng D, Huang D, Li W, Wang X. Disctinction of broken cellular wall *Ganoderma lucidum* spores and G. lucidum spores using FTIR microspectroscopy. *Spectrochim Acta A Mol Biomol Spectrosc.* 2012;97:667–672.
52. Gurunathan S, Han JW, Dayem AA, et al. Antibacterial activity of dithiothreitol reduced graphene oxide. *Journal of Industrial and Engineering Chemistry.* 2013;19(4):1280–1288.
53. Zhang HB, Zheng WG, Yan Q, et al. Electrically conductive polyethylene terephthalate/graphene nanocomposites prepared by melt compounding. *Polymer.* 2010;51(5):1191–1196.
54. Jin Y, Huang S, Zhang M, Jia M, Hu D. A green and efficient method to produce graphene for electrochemical capacitors from graphene oxide using sodium carbonate as a reducing agent. *Appl Surf Sci.* 2013;268: 541–546.
55. Liu P, Huang Y, Wang L. A facile synthesis of reduced graphene oxide with Zn powder under acidic condition. *Mater Lett.* 2013;91:125–128.
56. Lim HN, Huang NM, Loo CH. Facile preparation of graphene-based chitosan films: Enhanced thermal, mechanical and antibacterial properties. *J Non Cryst Solids.* 2012;358(3):525–530.
57. Si W, Wu X, Zhou J, et al. Reduced graphene oxide aerogel with high-rate supercapacitive performance in aqueous electrolytes. *Nanoscale Res Lett*. 2013;8(1):247.
58. Zhang W, He W, Jing X. Preparation of a stable graphene dispersion with high concentration by ultrasound. *J Phys Chem B*. 2010;114(32): 10368–10373.
59. Lotya M, Hernandez Y, King PJ, et al. Liquid phase production of graphene by exfoliation of graphite in surfactant/water solutions. *J Am Chem Soc*. 2009;131(10):3611–3620.
60. Dreyer DR, Park S, Bielawski CW, Ruoff RS. The chemistry of graphene oxide. *Chem Soc Rev.* 2010;39:228–240.
61. Schniepp HC, Li JL, McAllister MJ, et al. Functionalized single graphene sheets derived from splitting graphite oxide. *J Phys Chem B*. 2006;110(17):8535–8539.
62. Wang G, Wang B, Park J, Wang Y, Sun B, Yao J. Highly efficient and large-scale synthesis of graphene by electrolytic exfoliation. *Carbon.* 2009;47(14):3242–3246.
63. Kudin KN, Ozbas B, Schniepp HC, Prud'homme RK, Aksay IA, Car R. Raman spectra of graphite oxide and functionalized graphene sheets. *Nano Lett.* 2008;8(1):36–41.
64. Shen J, Li T, Shi M, Li N, Ye M. Polyelectrolyte-assisted one-step hydrothermal synthesis of Ag-reduced graphene oxide composite and its antibacterials properties. *Materials Science and Engineering: C*. 2012;32(7):2042–2047.
65. Alanyalıoğlu M, Segura JJ, Oró-Solè J, Casañ-Pastor N. The synthesis of graphene sheets with controlled thickness and order using surfactant-assisted electrochemical processes. *Carbon.* 2012;50(1):142–152.
66. Wang F, Zhang K. Reduced graphene oxide–TiO_2 nanocomposite with high photocatalystic activity for the degradation of rhodamine B. *J Mol Catal A Chem*. 2011;345(1–2):101–107.
67. Ferrari AC, Meyer JC, Scardaci V, et al. Raman spectrum of graphene and graphene layers. *Phys Rev Lett.* 2006;97(18):187401.
68. Li D, Müller MB, Gilje S, Kaner RB, Wallace GG. Processable aqueous dispersions of graphene nanosheets. *Nat Nanotechnol*. 2008; 3(2):101–105.
69. Stankovich S, Dikin DA, Dommett GH, et al. Graphene-based composite materials. *Nature.* 2006;442(7100):282–286.
70. Liu S, Zeng TH, Hofmann M, Burcombe E, Wei J, Jiang RR, et al. Antibacterial activity of graphite, graphite oxide, graphene oxide, and reduced graphene oxide: membrane and oxidative stress. *ACS Nano*. 2011; 5(9):6971–6980.
71. Compton OC, An Z, Putz KW, et al. Additive-free hydrogelation of graphene oxide by ultrasonication. *Carbon.* 2012;50(10): 3399–3406.
72. Yan J, Fan Z, Wei T, Qian W, Zhang M, Wei F. Fast and reversible surface redox reaction of graphene–MnO_2 composites as supercapacitor electrodes. *Carbon*. 2010;48(13):3825–3833.
73. Chang Y, Yang ST, Liu JH, et al. In vitro toxicity evaluation of graphene oxide on A549 cells. *Toxicology Lett*. 2011;200(3):201–210.
74. Sasidharan A, Panchakarla LS, Chandran P, Menon D, Nair S, Rao CN, et al. Differential nano-bio interactions and toxicity effects of pristine versus functionalized graphene. *Nanoscale.* 2011;3(6):2461–2464.
75. Mullick Chowdhury S, Lalwani G, Zhang K, Yang JY, Neville K, Sitharaman B. Cell specific cytotoxicity and uptake of graphene nanoribbons. *Biomaterials*. 2013;34(1):283–293.
76. Repetto G, del Peso A, Zurita JL. Neutral red uptake assay for the estimation of cell viability/cytotoxicity. *Nat Protoc*. 2008;3(7): 1125–1131.
77. Abdolahad M, Janmaleki M, Mohajerzadeh S, Akhavan O, Abbasi S. Polyphenols attached graphene nanosheets for high efficiency NIR mediated photodestruction of cancer cells. *Mater Sci Eng C Mater Biol Appl*. 2013;33(3):1498–1505.
78. Peng C, Hu W, Zhou Y, Fan C, Huang Q. Intracellular imaging with a graphene-based fluorescent probe. *Small.* 2010;6(15):1686–1692.
79. Miao W, Shim G, Lee S, Lee S, Choe YS, Oh YK. Safety and tumor tissue accumulation of pegylated graphene oxide nanosheets for co-delivery of anticancer drug and photosensitizer. *Biomaterials*. 2013;34(13):3402–3410.
80. Guo X, Mei N. Assessment of the toxic potential of graphene family nanomaterials. *J Food Drug Anal.* 2014;22:105–115.

81. Jaworski S, Sawosz E, Grodzik M, et al. *In vitro* evaluation of the ffects of graphene platelets on glioblastoma multiforme cells. *Int J Nanomedicine*. 2013;8:413–420.
82. Wang AX, Pu K, Dong B, et al. Role of surface charge and oxidative stress in cytotoxicity and genotoxicity of graphene oxide towards human lung fibroblast cells. *J Appl Toxicol.* 2013;33(10):1156–1164.
83. Duch MC, Budinger GRS, Liang YT, Soberanes S, Urich D, Chiarella SE, et al. Minimizing oxidation and stable nanoscale dispersion improves the biocompatibility of graphene in the lung. *Nano Lett.* 2011;11(12):5201–5207.